PHOTONICS Research

High-sensitivity integrated SiN rib-waveguide long period grating refractometer

Clement Deleau,[1,*] Han Cheng Seat,[1] Olivier Bernal,[1] and Frederic Surre[2]

[1]LAAS-CNRS, Université de Toulouse, CNRS, INP, Toulouse, France
[2]James Watt School of Engineering, University of Glasgow, Glasgow, UK
*Corresponding author: clement.deleau@laas.fr

Received 1 October 2021; revised 6 December 2021; accepted 15 December 2021; posted 16 December 2021 (Doc. ID 444825); published 1 February 2022

In this research, we demonstrate a high-sensitivity integrated silicon nitride long period grating (LPG) refractometer based on a rib waveguide with sinusoidally modulated width. While integrated LPG architectures typically achieve ultrahigh sensitivity only over a narrow optical bandwidth using a phase-matching turning-point optimization technique, our sensor exhibits a very high refractometric sensitivity that was designed to remain constant over a broad operational optical spectral bandwidth. The proposed design method relies on multi-modal dispersion tailoring that consists of homogenizing the spectral behaviors of both group and effective indices of the coupling modes. Experimental results are in agreement with numerical simulations, demonstrating not only a sensitivity reaching 11,500 nm/RIU but, more significantly, also that this sensitivity remains almost constant over a broad spectral range of at least 100 nm around 1550 nm. Additional advantages of the proposed sensor architecture encompass a low temperature sensitivity, down to −0.15 nm/K, and simplicity of the fabrication process. These results demonstrate the feasibility of chip-scale photonic integration to achieve both high sensitivity and large dynamic range of the proposed refractometer.

https://doi.org/10.1364/PRJ.444825

1. INTRODUCTION

Since their invention, refractometers have emerged as critical metrological tools extensively employed in industry for a broad range of applications, from chemical analysis [1] to temperature and strain sensing [2]. Refractometry-based sensors allow the estimation of the targeted physical or chemical parameter of interest via the optical measurement of its corresponding refractive index (RI). The inherent high versatility achievable among the wide variety of optical transducers contributes to driving research on refractometers toward increasingly higher sensitivities, resolution, and linearity. As the fundamental basis of many optical sensing solutions, refractometry has also been recently investigated for device implementation on the integrated photonic platform as a pathway to potentially achieve even higher performances while reducing the system's footprint [3]. Integrated silicon-based photonic sensors intrinsically benefit from major features such as electromagnetic immunity, compactness, and miniaturization, as well as their high flexibility of design [4]. These characteristics thus render the CMOS-compatible platform very attractive for high performance sensing schemes that require high resolution and precision while being cost effective. Integrated refractometers could be typically classified into five different categories: waveguide interferometers [5], resonators [6], photonic crystals [7], plasmonic devices [8], and diffraction gratings [9].

Long period gratings (LPGs) form a sub-family of the grating-based group. They consist of structures that operate on the exchange of energy between two or more co-propagative optical modes. This coupling is allowed by a periodic exchange of energy when the grating period and propagated wavelength satisfy a resonance condition. LPGs have been mainly investigated as fiber-based sensors because they allow optical energy to interact with the external environment by coupling a buried core mode to a leaking cladding mode [10] exposed to the external medium [11]. Any modification of the RI in the external environment results in a shift of a resonance wavelength. Their simplicity of fabrication using fiber tapering, irradiation, corrugation, inscription, or arc discharge has also rendered them attractive for mass fabrication. Moreover, LPGs have recently been subject to increasing interest for implementation in integrated photonics [12–16] due to their very high sensitivity potential, small footprints, and specific features that can be exploited on a design-flexible platform. In fact, when compared to typical interferometers or resonators, which exhibit periodic spectral patterns [17], LPGs offer the particular ability to create a localized spectral response while having similar performance potential. Obtaining such localized patterns is particularly advantageous, as it greatly facilitates the tracking of the LPG's spectral signature in highly sensitive refractometers.

In this work, we propose an integrated refractometric sensor operating on a long period waveguide grating (LPWG) implemented on a planar rib waveguide whose core width is sinusoidally modulated. Contrary to other optimization methods that generally improve the local sensitivity performance only around a narrow range of a few nanometers [14,18], we aim to show here that sensitivity can be uniformly enhanced over a broader spectrum by following certain design guidelines. This is performed on our structure by tailoring the effective indices of the coupled modes while simultaneously tuning the mode coupling strength. In Section 2, the LPWG sensing scheme is theoretically discussed and explained, and the design optimization method exploiting effective index (EI) tailoring is next described for sensitivity performance enhancement. In Section 3, the proposed architecture is detailed and modeled using modal analysis and eigenmode expansion (EME). The fabrication and characterization processes are then described in Section 4. Experimental results from optical refractometric measurements are subsequently presented and discussed in Section 5.

2. OPERATING PRINCIPLES

A. Long Period Grating Theory

LPGs are waveguide-based structures that employ periodic modulation to enable energy exchange between co-propagative optical modes. As each mode possesses a specific propagation constant and behavior, LPGs are designed to selectively couple modes at resonance wavelengths, as described by the phase-matching condition [19]

$$\Delta n_{\mathrm{eff},i,j}(\lambda_{\mathrm{res}}) \approx \frac{\lambda_{\mathrm{res}}}{\Omega}, \tag{1}$$

where $\Delta n_{\mathrm{eff},i,j} = n_{\mathrm{eff},i} - n_{\mathrm{eff},j}$, n_{eff_i} and n_{eff_j} are EIs of coupling modes i and j, respectively, Ω is the grating period, and λ_{res} is the resonance wavelength to achieve maximum coupling. For spectral features to appear around the resonance in the LPG's transmission spectrum, sufficient coupling strength and grating length are necessary to enable continuous coupling during the propagation of the injected mode. As described by the coupled mode theory [20] through numerous accepted LPG models, the continuous exchange of energy between modes around the resonance is periodic with respect to the LPG propagation length. Furthermore, when configured for specific sensor setups, this grating length has to be specifically set to enable complete mode coupling at resonance, so that energy is fully transferred between coupled modes. The coupling speed depends mainly on the coupling coefficients [20], which have previously been demonstrated to be mainly dependent on the optical field's modal superposition across the modulated area as well as on the modulation amplitude [15].

B. Long Period Grating as Refractometer

Perturbation of the optical system typically occurs through the interaction of the evanescent field of a mode with the target analyte, which results in modification of the propagation constants of the mode as a function of RI variation. As defined by Eq. (1), the central wavelength of the resonance λ_{res} largely depends on the EI difference of the coupling modes. Changes of LPG responses can subsequently occur by performing mode coupling to a perturbed optical mode. LPGs have mainly been implemented in fiber platforms for their capacity in unburying inner core fields and inducing interaction with an external medium to be sensed. Fiber LPG refractometers rely on the coupling between the fundamental core mode and a cladding mode; while the core mode's EI is relatively insensitive to external influence, selected cladding modes can, on the other hand, interact substantially with the external medium perturbation. The waveguide sensitivity of mode i, Γ_i, which represents sensitivity of the effective RI to the cladding index in evanescent optical waveguide sensors [21], can be expressed as

$$\Gamma_i(\lambda, n_{\mathrm{eff},i}) = \frac{\partial n_{\mathrm{eff},i}}{\partial n_{\mathrm{sens}}}(\lambda, n_{\mathrm{eff},i}), \tag{2}$$

where n_{sens} is the RI of the sensed region. Γ_i should not be confused with the sensed region's modal field overlap ratio, especially in high RI contrast waveguides [21]. Nevertheless, since Γ_i exhibits substantial correlation with the percentage of optical fields in the sensing region in most cases, it can thus be used as a tool to estimate the waveguide sensitivity.

Generally, LPG sensing systems rely on a wavelength interrogation technique. The sensitivity S_λ of the LPG is measured as spectral shifts of the resonance pattern per RI unit (RIU) of the sensed medium. Hence, the sensitivity equation can be calculated from Eq. (1) by applying a first-order Taylor series expansion [22], with respect to λ and n_{sens}, as detailed in Ref. [14], to result in

$$S(\lambda, i, j) = \lambda \frac{\Delta\Gamma_{i,j}(\lambda)}{\Delta n_{g,i,j}(\lambda)} \tag{3}$$

with $\Delta\Gamma_{i,j} = \Gamma_i(\lambda) - \Gamma_j(\lambda)$ and $\Delta n_{g,i,j} = n_{g,i} - n_{g,j}$, where $n_{g,i}$ denotes the modal group index (GI) of mode i, which can be expressed as $n_{g,i} = n_{\mathrm{eff},i} - \lambda \frac{\partial n_{\mathrm{eff},i}}{\partial \lambda}$ [23].

Two sensitivity improvement techniques have been previously employed in the design of integrated LPGs, namely, modal interaction optimization [12,15] and phase-matching turning-point (PMTP) optimization [14]. Modal interaction optimization relies on maximizing the sensing region's influence on the difference $\Delta\Gamma_{i,j}$ of the two coupling modes, while PMTP aims to minimize the GI difference $\Delta n_{g,i,j}$, thus significantly increasing spectral sensitivity, as illustrated by Eq. (3). In fact, by appropriately setting the grating period for coupling around the wavelength range of interest using Eq. (1), the sensitivity can be simplified into

$$S(\lambda, i, j) \approx \Delta\Gamma_{i,j}(\lambda) \cdot \Omega \cdot \gamma(\lambda), \tag{4}$$

where γ is known as the waveguide dispersion factor, defined as [22,24]

$$\gamma(\lambda) = \frac{\Delta n_{\mathrm{eff},i,j}(\lambda)}{\Delta n_{g,i,j}(\lambda)}. \tag{5}$$

Here, γ locally becomes infinite around the PMTP, whose associated wavelength can be obtained by solving $\Delta n_{g,i,j}(\lambda) = 0$, as illustrated in Fig. 1(a).

Optimization is typically performed by displacing the PMTP near the wavelength of interest using GI tuning to increase the γ contribution to overall spectral sensitivity. In practice, this is equivalent to engineering the chromatic dispersion of coupling modes to counteract or balance the difference

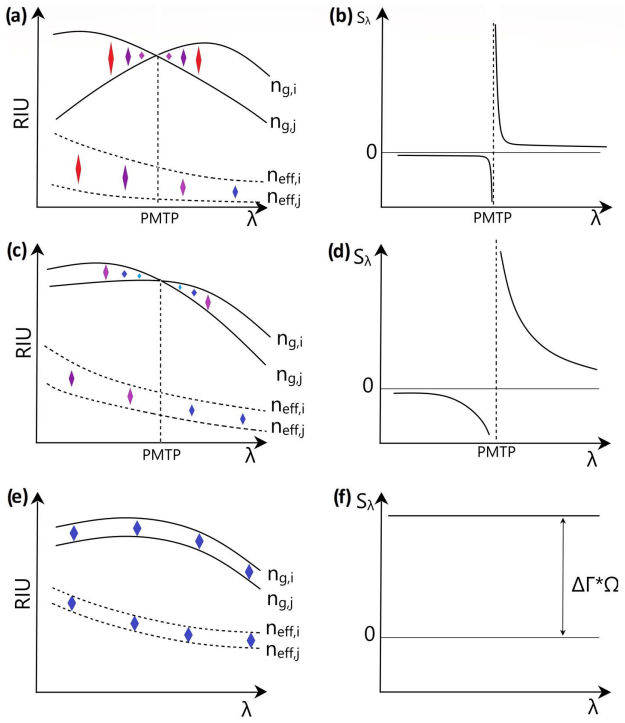

Fig. 1. Illustration of spectral sensitivity optimization behavior. (a), (c), (e) Different propagation constant spectral profiles and (b), (d), (f) subsequent expected sensitivity behavior versus wavelength.

between the EIs of coupling modes within the spectral window of interest. A notable problem with PMTP optimization is that the sensitivity enhancement significantly drops as the resonance shifts away from the PMTP, as illustrated in Fig. 1(b), thereby considerably reducing the RI sensing range. This is due to the high chromatic dispersion difference between modes that causes $\Delta n_{g,i,j}$ to greatly vary with λ, thus causing the sensitivity to collapse.

To circumvent this issue, we propose in this research another method based on the tailoring of the coupling modes so that the coupled modes' chromatic dispersion behaviors and EIs could be brought as close as possible. This should result in a sensitivity improvement similar to the PMTP method, with the additional characteristic of the resulting sensitivity response remaining almost constant over a much wider wavelength measurement range, as illustrated in Figs. 1(e) and 1(f). In this case, γ becomes nearly constant and close to one, and the sensitivity enhancement is mainly derived from the extended grating period Ω that is needed for coupling modes with close EIs, as shown in Eq. (1).

In addition to the sensitivity, the full-width at half-maximum (FWHM) can be utilized for comparing refractometric schemes, as it can provide insight on the resolution achievable in tracking both the induced resonance location and shift, thus accounting for the sensor performance. FWHM can be estimated as follows [25]:

$$\mathrm{FWHM}(\lambda_{\mathrm{res}}) \approx \frac{0.8\lambda_{\mathrm{res}}^2}{L_{\mathrm{opt}} \cdot \Delta n_{g,i,j}(\lambda_{\mathrm{res}})}, \tag{6}$$

where L_{opt} is the optimal LPG length for which full coupling is obtained at λ_{res}. Shaping of the spectral widths of the LPGs' resonance patterns can thus be performed by engineering the grating profile, coupling parameters, and grating length.

C. Proposed Structure

The proposed structure consists of a partially covered silicon nitride (SiN) hybrid rib–strip waveguide of RI $n_{\mathrm{SiN}} = 1.97$ whose core width is modulated to form an LPG as illustrated in Fig. 2. SiN on silicon oxide technology is chosen for its simplicity of fabrication and patterning, and for its relatively low index contrast in comparison with silicon on insulator (SOI), which facilitates modal tailoring. Also, rib waveguides possess significant advantages when employed for the design of LPWGs. As previously reported in Ref. [13], tailoring of the rib etch dimensions can enable the structure to support a fundamental mode confined within the waveguide core region together with higher-order modes spread out over the slab region. The optical fields of the propagating fundamental HE1 mode and the higher-order odd slab mode HE7 are simulated and plotted in Fig. 3. As the optical fields of both core and slab modes are partially overlapping in the modulated region, the field product integral at the modulated interface is non-null for odd modes. This is necessary to enable energy coupling between modes near λ_{res} during mode propagation, as previously illustrated in Ref. [15]. Moreover, since the optical profiles of the coupling modes are principally confined in the same material, two major features that can be exploited for sensing can be expected. First, as will be shown in Section 3.C, an intrinsic property of the rib structure is that it can support modes whose EIs and GIs can potentially be induced to be very close and to behave similarly over a broad wavelength range, thus favoring our optimization scheme. Second, since the LPG resonance relies on a differential mechanism as described by Eq. (1), both modes are expected to be almost equally affected by temperature or material dispersion due to their co-propagation in the same material: the structure is inherently less prone to temperature cross talk [13,26], and material dispersion can be neglected in the simulated models. In addition, the waveguide grating modulation is designed to be continuous along the core section width, which further reduces propagative losses due to optical leakage that would otherwise occur in typical binary-etched gratings, as shown in Ref. [14]. It further facilitates the theoretical analysis of mode coupling via coupling local mode theory [20], which is exact only in the case of

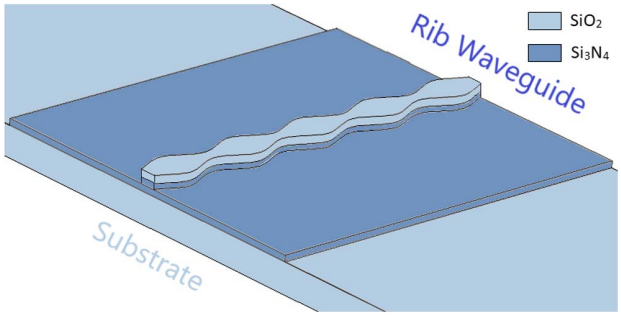

Fig. 2. Illustration of the implemented rib waveguide LPG structure with sinusoidally modulated width.

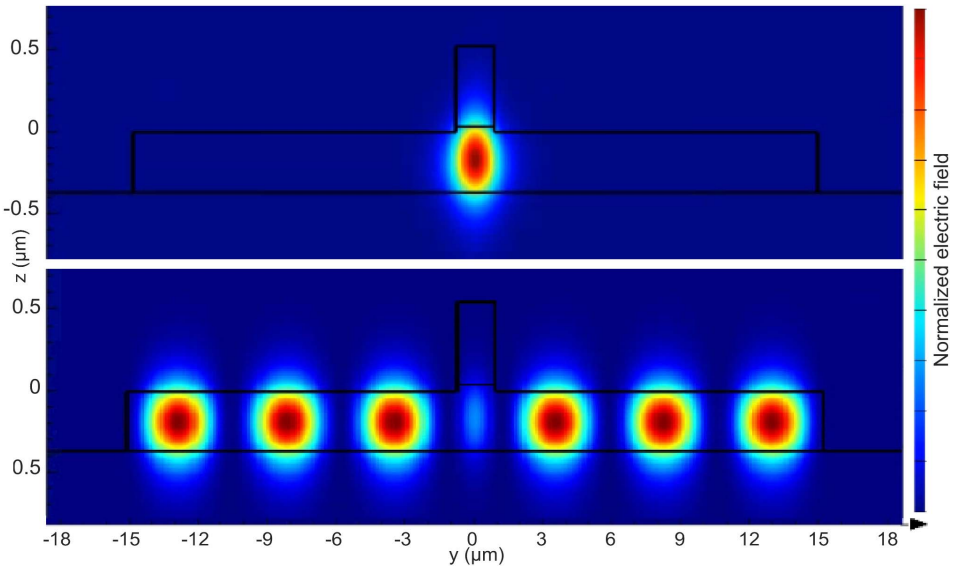

Fig. 3. Simulated mode profiles for a rib LPWG: HE1 (top) and HE7 (bottom).

"slowly varying waveguide approximations," thereby allowing to accurately model the LPWG for optimization purposes, as demonstrated in Ref. [15]. Nevertheless, converting our sinusoidally modulated LPWG to a binary one remains possible. The last particularity of our structure is that the core region is partially covered by silicon oxide (SiO_2), thus attenuating the sensitivity of the fundamental mode in the core to perturbations in the sensing region while the slab modes, on the contrary, substantially interact with this region. The SiO_2 layer is efficiently implemented during the fabrication process by using a specific resist without requiring any supplementary process step, as will be detailed in the next section.

3. DESIGN OPTIMIZATION AND LPWG ARCHITECTURE

A standard 400 nm SiN core thickness, h_{core}, has been chosen to facilitate optical injection into the photonic chip via grating couplers as well as for relatively unconstrained fundamental mode propagation. Further, as illustrated in Fig. 4, the remaining rib waveguide parameters, such as slab thickness, h_{slab}, which depends on the etch depth e, core width w_{core}, and slab width w_{slab}, have been optimized with respect to the following guidelines.

1. The EIs of the core and slab modes must be in very close proximity to induce high sensitivity and significantly extend the measurement range.
2. The modal interaction with the external region must be as strong as possible for the slab modes and almost null for the core mode.
3. The overlapping of the modal fields at the modulated interface must be tuned for coupling rate optimization [15,20].
4. The difference in chromatic dispersion between the two coupling modes is small in the spectral region of interrogation.

The following subsections describe the LPWG structural parameters that are chosen. In this research, we employ Lumerical's mode solver to simulate the rib LPWG [27] for which the mesh resolution has been set at 1 nm in the core region and surrounding interfaces. Note that both metal and perfectly matched layer boundary conditions lead to identical results, as they are positioned sufficiently far from the waveguide.

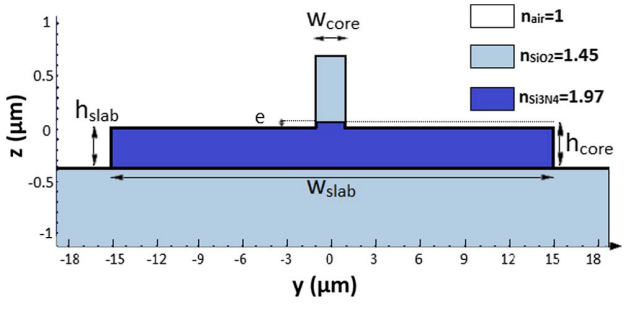

Fig. 4. LPG cross-sectional profile.

A. SiO_2 Strip

As previously described, $\Delta\Gamma_{i,j}$ can be increased by controlling the optical field overlap of the respective coupling modes to the sensing region. This is performed by minimizing the optical leakage of the fundamental mode into the sensing region while enabling slab modes to expand in the external environment. To minimize the core mode sensitivity to the sensing region $\Gamma_{HE1}(\lambda)$, a strip of SiO_2 is deposited on top of the core region. Here, Γ_{HE1}, as evaluated by simulation, has been lowered to $\approx$0.02. Additionally, as described in more detail in Section 4, during the fabrication process, the SiO_2 strip can also be advantageously used as the mask for patterning the modulated waveguide, thereby reducing further the required number of process steps. A minimum strip thickness of 0.5 μm is determined to be sufficient to prevent additional leakage.

B. Slab Thickness

We observe that the etch depth, e, appears to be the most influential parameter on the LPWG behavior. As the slab region becomes thinner, the slab mode's evanescent field expands into the cladding and substrate regions. It first enhances the sensed region's influence on the propagation constants of the slab modes by increasing $\Gamma_{\text{slabmodes}}$ because a higher proportion of the modal field now interacts with the sensed region. However, if e is too small, the fundamental mode will no longer be confined in the core region and will, instead, start leaking horizontally into the slab region, thereby increasing Γ_{coremode}. Second, e is the main contributor to the EI difference between the slab–core modes, where stronger vertical confinement will cause the EIs of the slab modes to further decrease. Since they are already inherently lower than that of the core mode, it would result in a lower LPG spectral sensitivity. Last, e also significantly influences the LPG's coupling strength since the latter depends on the modulated area (which, in turn, is proportional to e) [15,20]. Figure 5 shows the influence of e on both $\Delta n_{\text{eff,HE}_7,\text{HE}_1}$ and $\Delta\Gamma_{\text{HE}_7,\text{HE}_1}$. As a trade-off among Γ coefficients, EIs, and coupling coefficient optimization, the slab thickness h_{slab} is chosen to be 365 nm.

C. Slab Width

Mode calculations suggest that the EIs of slab modes tend to increase and approach the EI of the fundamental mode with increasing slab width (w_{slab}). However, since large w_{slab} will also spread the slab's mode field, the electric field superposition at the modulated interface will tend to decrease, thereby reducing the amplitude of the coupling coefficient and, consequently, increasing the required sensor length. A 30 μm wide slab is found to be a good compromise to enable full optical coupling to the first slab modes over a millimeter-scale propagation length. Figure 6 illustrates the simulated propagation constant EIs and GIs of modes HE1 and HE7, respectively, in the NIR spectral band (from ≈1.3 to 1.8 μm). It can be observed that the coupling modes' EIs behave very similarly so that $\Delta n_{g,i,j}$ and $\Delta n_{\text{eff},i,j}$ are relatively small and constant over a large wavelength band, similar to Figs. 1(e) and 1(f). These suggest that both very high sensitivities up to $S_\lambda = 10{,}000$ nm/RIU [as demonstrated by Eq. (3)] at a relatively constant level over the entire C-band could simultaneously be attained.

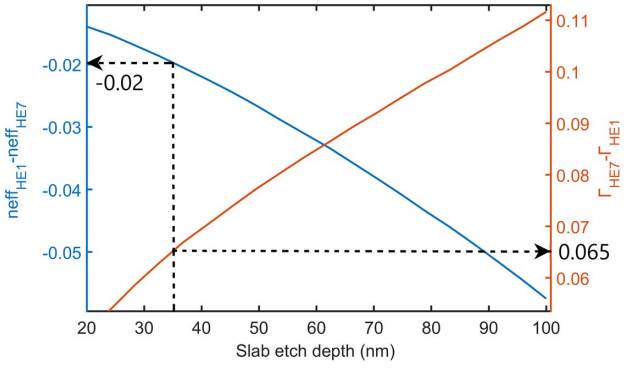

Fig. 5. Coupling modes' EI difference and waveguide sensitivity Γ difference versus slab etch depth with $w_{\text{slab}} = 30$ μm and $w_{\text{core}} = 1.65$ μm at 1550 nm. Etch depth is set at $e = 35$ nm and $h_{\text{slab}} = 365$ nm. Dashed lines: chosen etch depth and corresponding Δn_{eff} and $\Delta\Gamma$.

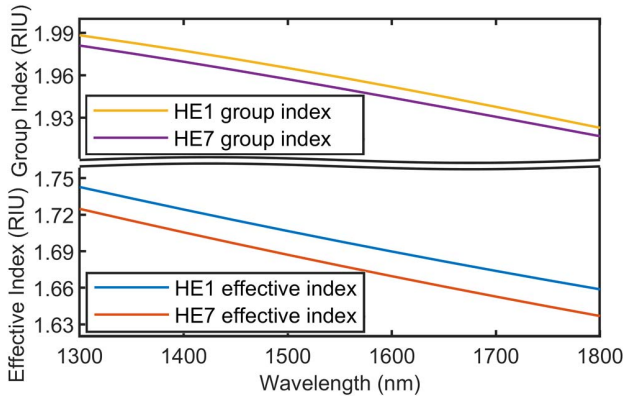

Fig. 6. Simulated effective and group indices of modes HE1 and HE7 showing similar dispersion with $e = 35$ nm, $w_{\text{core}} = 1.65$ μm, and $w_{\text{slab}} = 30$ μm.

D. Core Width

The core width is found to have little effect on the EIs of both core and slab modes when tuned between 1 and 3 μm. Nevertheless, two criteria have to be taken into account for the proper design of the LPWG. First, single mode propagation within the core region has to be ensured to minimize Γ_{coremode} and maximize $\Gamma_{\text{slabmodes}}$. Second, the core width also determines the geometrical location of the modulated interfaces on the slab surface. This parameter has to be optimized to obtain a specific modal field superposition for a particular coupling strength to be achieved. Furthermore, as demonstrated by Eqs. (3) and (6), the FWHM of the resonance can be determined with L_{opt} and the propagation constants. Hence, to facilitate experimental measurements, an FWHM lower than or equal to 25 nm has been estimated as the maximum measurable FWHM permissible to accurately observe the coupling spectra for different external indices, as our apparatus' measurement spectral window is only approximately 100 nm wide. Figure 7 illustrates the influence of the core width on the main coupling strength parameter, $\int_e E_{\text{HE1}} \cdot E_{\text{HE7}}\, dz$, which can further be used to estimate the expected coupling length for a given modulation amplitude of 0.15 μm, for example, as previously demonstrated in Ref. [15]. The average width of the core, w_{core}, is set to 1.65 μm to achieve a 25 nm wide spectral dip with full mode coupling, corresponding to a grating length of 7.5 mm.

E. LPWG Period and Length

As described by Eq. (1), when the EIs of the coupling modes are closer, the LPWG period greatly increases. To couple the HE1 and HE7 modes around 1550 nm, whose EIs are found to be, respectively, 1.693 and 1.673, the period has to be set to ≈77.5 μm. Here, EME is employed as an efficient technique to model mode propagative periodic structures [28], as previously demonstrated in Ref. [15]. In this work, one single period of the LPWG architecture is first sliced into 20 partitions along the propagation axis. The modes and field overlaps are then calculated for each local cross section. Subsequently, after a numerical reconstruction of the LPWG profile along the

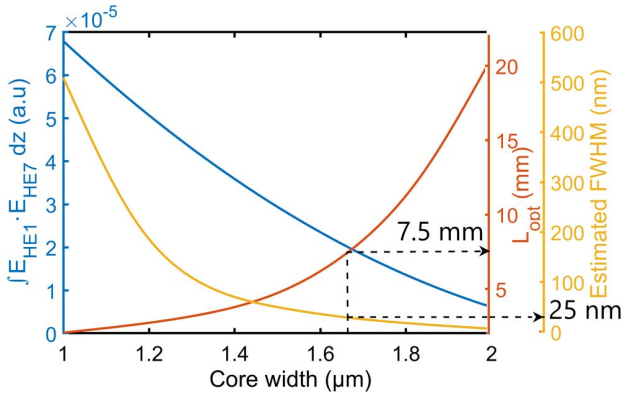

Fig. 7. Coupling parameter and estimated full coupling length versus core width with $e = 35$ nm and $w_{slab} = 30$ μm at 1550 nm. w_{core} is set at 1.65 μm. Dashed lines: chosen core width and corresponding coupling length L_{opt} and FWHM.

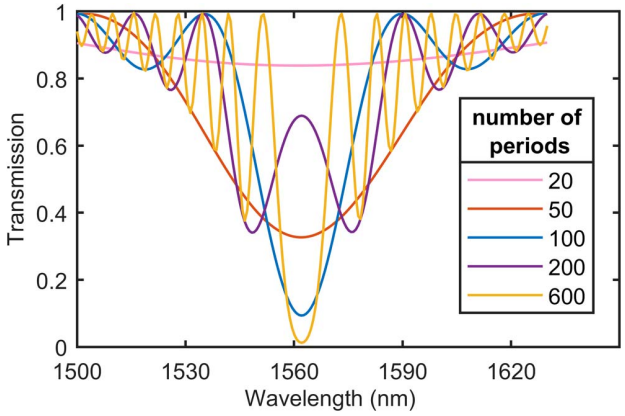

Fig. 8. Resonance spectra simulated with EME for different LPWG lengths with a period of 77.5 μm, $e = 35$ nm, $w_{slab} = 30$ μm, and $w_{core} = 1.65$ μm.

propagation axis, the continuous optical coupling in the LPWG over the propagation length is calculated with successive optical energy distribution by superposition of the scattering matrices. Figure 8 plots the simulated output spectra for different grating lengths, illustrating a simulated coupling length very similar to the calculated length. The model demonstrates a 25 nm FWHM that can be obtained over 100 periods, which is similar to the designed grating length of 7.5 mm.

4. FABRICATION

A. Layout

To facilitate optical injection into the photonic chip, standard grating couplers are used, as they enable easy characterization of the optical structures [4]. Fundamental mode coupling in the rib waveguide is then performed using 50 μm long strip–rib tapers at both ends of the LPWG [29]. Since fabrication defaults due to both variations of material RIs and geometrical dimensions of the patterned waveguides, and also high sensitivity ($S_\lambda > 10{,}000$ nm/RIU), are expected, several LPWGs of slightly different periods are fabricated to optimize the chances to obtain the coupling resonance within our measurement spectral range. Figure 9 illustrates the layout of the fabricated photonic chip, including LPWGs and grating couplers that have been designed.

B. Process

As illustrated in Fig. 10, a SiO_2 layer of approximately 2 μm thickness is first deposited on a pre-cleaned Si wafer by plasma-enhanced chemical vapor deposition (PECVD). A 400 nm thick SiN core layer is next deposited on top of the SiO_2 film, also by PECVD. The index of this core is measured by ellipsometry to be $n_{core} \sim 1.97$. The SiO_2 top strip is then fabricated using electron-sensitive hydrogen silsesquioxane resist (HSQ), whose constitution is found to be very similar to SiO_2 after curing, with an RI of 1.37 [30]. Moreover, the resist is also used as the etching protective layer for patterning the core waveguide and grating couplers. Subsequently, electron-sensitive MaN2405 resin is deposited by spin coating, followed by an Electra92 resin layer used for electronic charge dissipation during electron-beam lithography with a RAITH150 E-beam writer. This lithography step is used to pattern the slab region of the waveguide. The main E-beam exposure parameters, namely, acceleration voltage, beam current, step size, and dose, are respectively 20 kV, 37 pA, 10 nm, and 112 μC/cm^2 for MaN2405 resist, and 30 kV, 325 pA, 10 nm, and 375 μC/cm^2 for HSQ. After the resist development, the SiN layer (thickness ~400 nm) is etched using reactive ion etching (RIE) to obtain grating couplers and slab waveguides that are fully delineated. The remaining MaN2405 resist is removed using pirhana solution followed by plasma O_2 cleaning without affecting the SiO_2 strip generated from HSQ or the unetched SiN layer. Finally, a 35 nm etch is performed on the slab region of the rib waveguide using the SiO_2 strip as the layer mask. This particular process has two advantages: (i) the core and grating mask layer are also used as the protective strip of the core region to enhance sensitivity, and (ii) the fully etched grating couplers and partially etched rib-waveguide core region are patterned with the same mask, thereby reducing

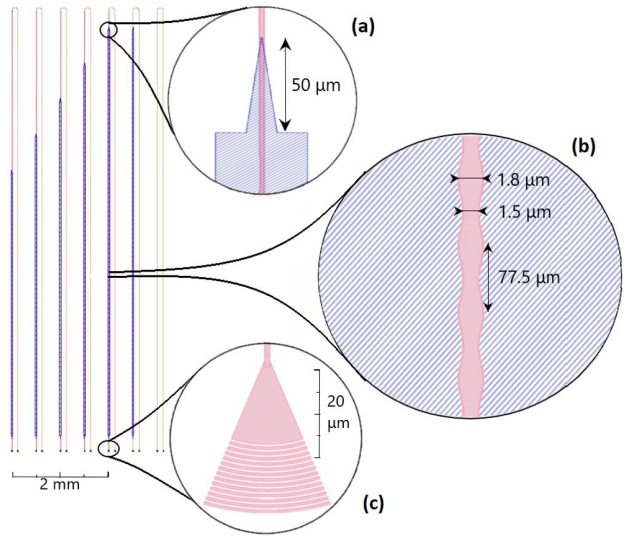

Fig. 9. Layout of the designed photonic chip showing (a) strip–rib converter, (b) LPWG, and (c) grating coupler.

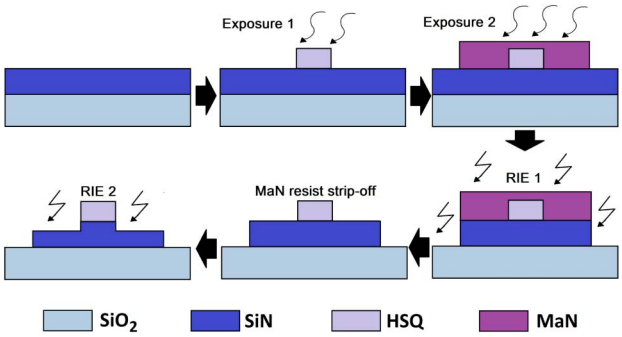

Fig. 10. Illustration of LPWG fabrication process.

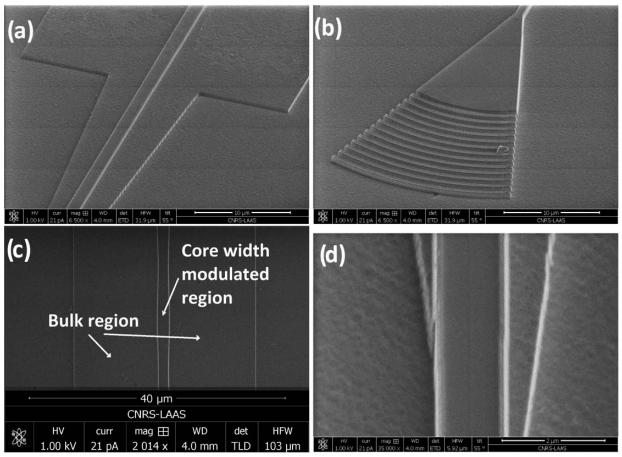

Fig. 11. SEM pictures of photonic circuit components: (a) strip–rib converter; (b) grating coupler, (c) LPWG section, and (d) minor misalignment between strip and rib waveguides shown here at the beginning of the tapering region for the sake of clarity.

possible mismatch during the strip–rib fundamental mode conversion.

C. Structure Characterization

The rib LPWGs are first physically characterized using a scanning electron microscope (SEM) as seen in Fig. 11(d). A transverse shift of 600 nm is observed on the second patterned layer. This 600 nm off-alignment is reintroduced into the simulation model and found to cause a minor resonance shift of ~20 nm with ~3% sensitivity variation.

5. EXPERIMENTAL RESULTS

A. Experimental Setup

The experimental setup for optical characterization consists of a Santec TSL550 tunable laser source, a fiber array mounted on a motorized linear stage driven by a dedicated LabVIEW program, and an optical powermeter, as illustrated in Fig. 12. The injection and recovery of the interrogating light into the photonic circuit is obtained by positioning the fiber array on top of a chip-integrated grating coupler pair. The injected laser wavelength is next scanned over the spectral region of interrogation from which the transmission spectrum is then measured. The transmission spectra of the LPWGs are obtained after de-embedding the transmitted signal to isolate both the LPWG's and tapers' spectral contributions from those of the grating couplers, tunable laser output, and lead-in/lead-out waveguides. It is first observed during optical characterization of the LPWGs that the background loss of ~7 dB, which includes contribution from each taper, is slightly lower for rib waveguides relative to a control sample based on strip waveguides. This can be attributed to the overall reduction of the sidewall surface area in the rib waveguides, which alleviates the roughness-induced refraction losses during optical propagation.

B. Sensitivity

Commercially available liquids of calibrated RIs from Cargill are employed and mixed into different proportions to simulate

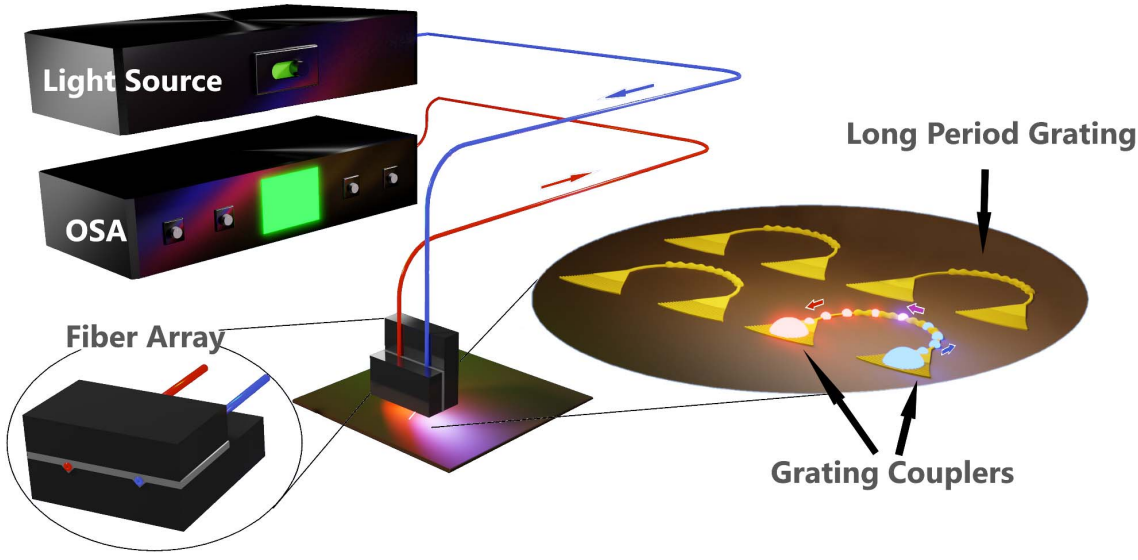

Fig. 12. Illustration of the experimental photonic characterization setup.

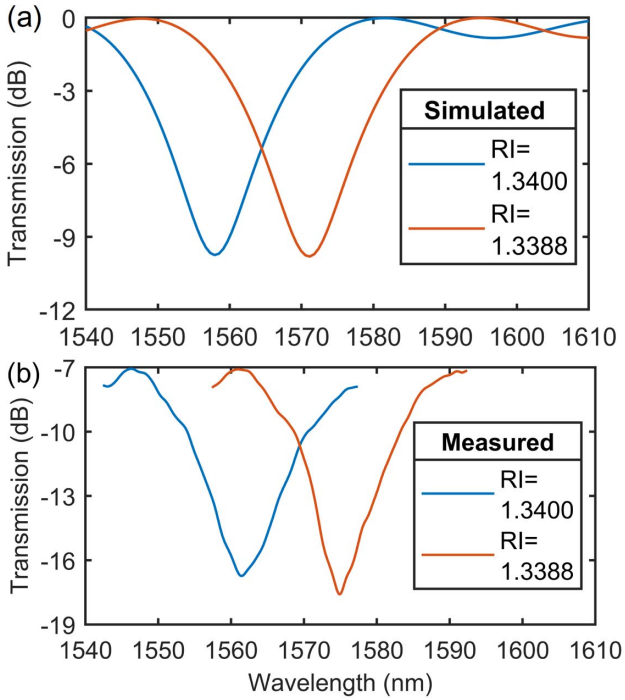

Fig. 13. (a) Simulated and (b) experimentally measured normalized resonance spectra at surface RIs of 1.3388 and 1.34.

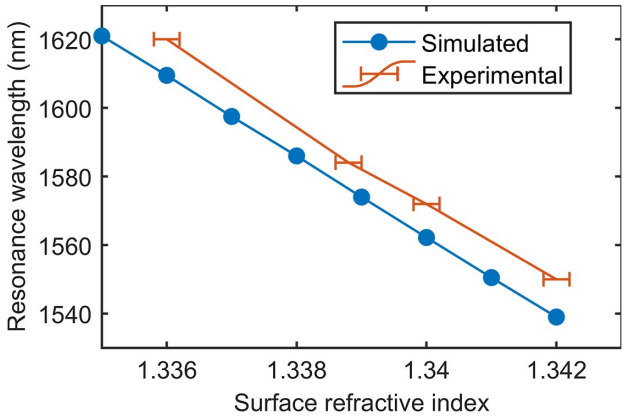

Fig. 14. Simulated and measured resonance wavelength of LPWGs obtained for different surface RIs.

indices varying between 1.33 and 1.35 RIUs. These RIs are first measured using a commercial Hanna HI 96801 refractometer with a resolution of 0.2 mRIU. The optical liquids are then deposited on top of the chip to induce RI variations in the LPWG resonance, which is subsequently tracked over a spectral window of 100 nm. Resonance features observed during the optical characterization of an LPWG with a 77.5 μm period, as shown in Fig. 13, exhibit a 3 dB bandwith of 25 nm and an extinction ratio of 10–12 dB, which are very similar to the simulated values. Figure 14 plots the simulated and experimental resonance wavelength of the LPWG against the analyte's RI, from which the sensitivity calculated as the slope can be extracted. Here, the experimentally measured sensitivity is estimated to be $S_\lambda \approx 11{,}500$ nm/RIU and highly stable over 100 nm (limited by the SANTEC TSL550 measurement range), in good agreement with the simulated value.

Table 1 summarizes the sensitivities and specific properties of our proposed structure in comparison with previously reported fabricated LPWGs. Other LPWG designs based on waveguide sensitivity enhancement [12,16] or the PMTP optimization technique [14] exhibit either limited sensitivity enhancement or measurement range, respectively. On the other hand, our proposed sensor demonstrates ultrahigh sensitivity that, more significantly, is found to remain constant over a broad measurement range.

C. Temperature Dependence

To study the influence of temperature on our structure, the thermo-optic coefficients of SiN and SiO_2 are first determined to be 2.45×10^{-4} RIU/K and 9.5×10^{-5} RIU/K, respectively [31]. These are then introduced into our simulation model from which a very low temperature sensitivity of 150 pm/K is obtained. This low value is to be expected since the coupled modes travel in the same materials and are thus subject to the same influence. To experimentally study the temperature sensitivity of our sensor, the temperature of the laser mount is tuned using a Thorlabs thermo-electric cooler (TEC) with a 0.02°C precision. Nevertheless, it is impossible here to directly measure the temperature sensitivity of the sensor in free space (i.e., without an external "cladding" medium), as the mode resonance would then not fall within the limits of the target spectral range around 1550 nm. To correctly measure this sensitivity without exceeding the spectral limits, a calibrated RI liquid with a pre-characterized temperature dependence is applied on the LPWG surface. The resonance wavelength shift due to the liquid's RI variation induced by the temperature

Table 1. Comparison with Other Fabricated LPWGs

References	Material	Structure Type	LPG Length (μm)	Measured Sensitivity (nm/RIU)	FWHM (nm)	Period (μm)
[16]	Silicon nitride	Polymer waveguide coupling	1000	240–900	5	10
[13]	BK-7 glass	Rib waveguide	1915	240	3	180
[12]	Silicon nitride	Strip–slot waveguide coupling	2000	1970	7	15.1
[14]	Silicon	Asymmetric strip waveguide	1500	5078	20–30	7.8
Our work	**Silicon nitride**	**Rib waveguide**	**7750**	**11,500**	**25**	**77.5**

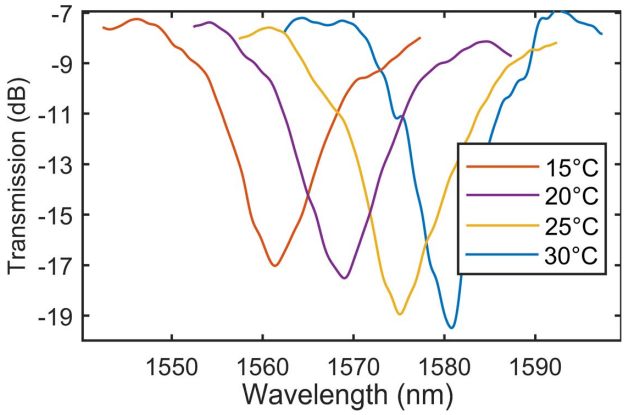

Fig. 15. Experimental wavelength resonance pattern shifts with temperature of the LPWG.

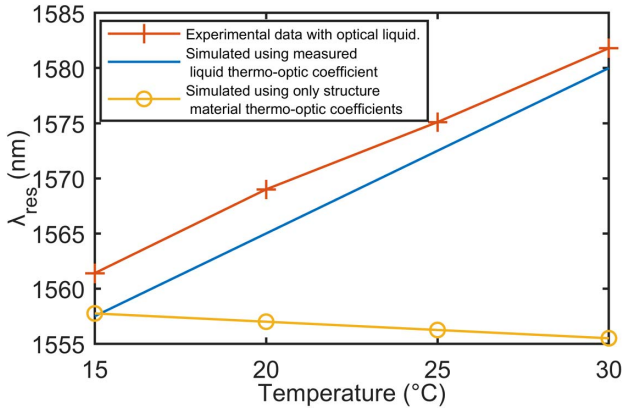

Fig. 16. Simulated and measured resonance wavelength variations versus temperature of the LPWG.

variation is finally subtracted from the combined total resonance shift (from both the RI liquid and LPWG sensor) to obtain the intrinsic temperature dependence of the LPWG structure (Figs. 15 and 16). The measured temperature sensitivity is found to corroborate the simulated value, which predicts a low intrinsic LPWG temperature dependence of ~150 pm/K.

6. CONCLUSION

Integrated refractometers are under intense investigation as the current state of the art in nano-fabrication lends unprecedented flexibility in the design of wavelength-scale complex photonic structures. In this paper, we proposed a novelty integration of a structure typically implemented on fiber platforms, i.e., the LPG. Indeed, alongside interferometers, LPWGs are photonic structures that benefit most from current advances in waveguide manufacturing technology [32], as their performance ultimately scales to the propagation length. However, unlike high-sensitivity interferometers for which the analysis of their spectral shift is complicated by the output spectral periodicity, LPWGs, on the other hand, which present localized spectral patterns, are promising candidates for constructing ultrahigh performance refractometers. The proposed structure, consisting of a rib-waveguide LPG, has been designed, fabricated, and characterized. A very high sensitivity of $S_\lambda \approx 11{,}500$ nm/RIU together with a figure of merit (FOM $= S_\lambda$/FWHM) of approximately 400 has been measured over a wide spectral window of 100 nm, in agreement with theoretically calculated and simulated values. This design has been found to demonstrate the efficiency of EI tuning and could, additionally, be further combined with other methods to potentially increase the sensitivity to values hitherto unmatched on the integrated platform. In this work, we also demonstrated the significant design capabilities of rib LPWGs, which exhibited critical features such as minimal temperature cross talk and simplicity of fabrication. Finally, an ongoing study further suggests that certain types of similar waveguides can possess inherent dispersive behaviors that allow their sensitivity to be multiplied by one to two orders without any reduction in sensitivity stability over the entire measurement range. Results from our new study shall be published in a future paper.

Funding. Institut National Polytechnique de Toulouse (Toulouse Tech Interlabs 2019).

Acknowledgment. All fabrication and characterization of the integrated photonic long period waveguide gratings were supported by both TTIL 2019 (Toulouse Tech Interlabs) and RENATECH (French Network of Technology Platforms) within LAAS-CNRS cleanroom infrastructure. The authors thank A. Lecestre, F. Carcenac, J.-B. Doucet, and L. Mazenq for their technical assistance with the fabrication and characterization process of the photonic integrated circuits.

Disclosures. Other than a patent filing application that is in progress on certain elements of this work, the authors declare no conflicts of interest.

Data Availability. Data underlying the results presented in this paper are not publicly available at this time but may be obtained from the author upon reasonable request.

REFERENCES

1. A. Urrutia, I. Del Villar, P. Zubiate, and C. Zamarreño, "A comprehensive review of optical fiber refractometers: toward a standard comparative criterion," Laser Photon. Rev. **13**, 1900094 (2019).
2. M. Ramakrishnan, G. Rajan, Y. Semenova, and G. Farrell, "Overview of fiber optic sensor technologies for strain/temperature sensing applications in composite materials," Sensors **16**, 99 (2016).
3. E. Luan, H. Shoman, D. M. Ratner, K. C. Cheung, and L. Chrostowski, "Silicon photonic biosensors using label-free detection," Sensors **18**, 3519 (2018).
4. L. Chrostowski and M. Hochberg, *Silicon Photonics Design: From Devices to Systems* (Cambridge University, 2015).
5. X. Guan and L. H. Frandsen, "All-silicon interferometer with multimode waveguides for temperature-insensitive filters and compact biosensors," Opt. Express **27**, 753–760 (2019).
6. S. Chandran, R. K. Gupta, and B. K. Das, "Dispersion enhanced critically coupled ring resonator for wide range refractive index sensing," IEEE J. Sel. Top. Quantum Electron. **23**, 424–432 (2017).

7. P. Xu, J. Zheng, J. Zhou, Y. Chen, C. Zou, and A. Majumdar, "Multi-slot photonic crystal cavities for high-sensitivity refractive index sensing," Opt. Express **27**, 3609–3616 (2019).
8. E. Chatzianagnostou, A. Manolis, G. Dabos, D. Ketzaki, A. Miliou, N. Pleros, L. Markey, J.-C. Weeber, A. Dereux, B. Chmielak, A.-L. Giesecke, C. Porschatis, P. J. Cegielski, and D. Tsiokos, "Scaling the sensitivity of integrated plasmo-photonic interferometric sensors," ACS Photon. **6**, 1664–1673 (2019).
9. X. Wang, J. Flueckiger, S. Schmidt, S. Grist, S. T. Fard, J. Kirk, M. Doerfler, K. C. Cheung, D. M. Ratner, and L. Chrostowski, "A silicon photonic biosensor using phase-shifted Bragg gratings in slot waveguide," J. Biophoton. **6**, 305–828 (2013).
10. E. Simões, I. Abe, J. Oliveira, O. Frazão, P. Caldas, and J. Pinto, "Characterization of optical fiber long period grating refractometer with nanocoating," Sens. Actuators B **153**, 335–339 (2011).
11. H. Hu, C. Du, Q. Wang, X. Wang, and Y. Zhao, "High sensitivity internal refractive index sensor based on a photonic crystal fiber long period grating," Instrum. Sci. Technol. **45**, 181–189 (2016).
12. Q. Liu, Z. Gu, M. K. Park, and J. Chung, "Experimental demonstration of highly sensitive optical sensor based on grating-assisted light coupling between strip and slot waveguides," Opt. Express **24**, 12549–12556 (2016).
13. U. Tripathi and V. Rastogi, "Temperature insensitive long period waveguide gratings in rib waveguide," Optik **186**, 15–21 (2019).
14. J. Høvik, M. Yadav, J. W. Noh, and A. Aksnes, "Waveguide asymmetric long-period grating couplers as refractive index sensors," Opt. Express **28**, 23936–23949 (2020).
15. C. Deleau, H. Seat, H. Tap, F. Surre, and O. Bernal, "Integrated silicon nitride horizontal long period grating for refractometric gas sensing applications," in *IEEE International Instrumentation and Measurement Technology Conference (I2MTC)* (2020), pp. 1–6.
16. C. Deleau, H. C. Seat, H. Tap, F. Surre, and O. D. Bernal, "Integrated width-modulated sin long period grating designed for refractometric applications," J. Lightwave Technol. **39**, 4820–4827 (2021).
17. M. Kitsara, K. Misiakos, I. Raptis, and E. Makarona, "Integrated optical frequency-resolved Mach-Zehnder interferometers for label-free affinity sensing," Opt. Express **18**, 8193–8206 (2010).
18. R. Wong, D. Hu, M. Ibsen, and P. Shum, "Optical fibre long-period grating sensors operating at and around the phase matching turning point," in *Applications of Optical Fibers for Sensing* (IntechOpen, 2019), https://www.intechopen.com/chapters/63687.
19. H. Taylor and A. Yariv, "Guided wave optics," Proc. IEEE **62**, 1044–1060 (1974).
20. A. W. Snyder and J. Love, *Optical Waveguide Theory* (Springer, 2012).
21. G. Veldhuis, O. Parriaux, H. Hoekstra, and P. Lambeck, "Sensitivity enhancement in evanescent optical waveguide sensors," J. Lightwave Technol. **18**, 677–682 (2000).
22. T. MacDougall, S. Pilevar, C. Haggans, and M. Jackson, "Generalized expression for the growth of long period gratings," IEEE Photon. Technol. Lett. **10**, 1449–1451 (1998).
23. E. A. J. Marcatili, "Modal dispersion in optical fibers with arbitrary numerical aperture and profile dispersion," Bell Syst. Tech. J. **56**, 49–63 (1977).
24. X. Shu, L. Zhang, and I. Bennion, "Sensitivity characteristics of long-period fiber gratings," J. Lightwave Technol. **20**, 255–266 (2002).
25. L. Rindorf and O. Bang, "Sensitivity of photonic crystal fiber grating sensors: biosensing, refractive index, strain, and temperature sensing," J. Opt. Soc. Am. B **25**, 310–324 (2007).
26. Q. Liu, K. S. Chiang, and K. P. Lor, "Condition for the realization of a temperature-insensitive long-period waveguide grating," Opt. Lett. **31**, 2716–2718 (2006).
27. http://www.lumerical.com.
28. D. Gallagher and T. Felici, "Eigenmode expansion methods for simulation of optical propagation in photonics - pros and cons," Proc. SPIE **4987**, 69–82 (2003).
29. T. Aalto, K. Solehmainen, M. Harjanne, M. Kapulainen, and P. Heimala, "Low-loss converters between optical silicon waveguides of different sizes and types," IEEE Photon. Technol. Lett. **18**, 709–711 (2006).
30. C. W. Holzwarth, T. Barwicz, and H. I. Smith, "Optimization of hydrogen silsesquioxane for photonic applications," J. Vac. Sci. Technol. B **25**, 2658–2661 (2007).
31. A. Arbabi and L. Goddard, "Measurements of the refractive indices and thermo-optic coefficients of Si_3N_4 and SiO_x using microring resonances," Opt. Lett. **38**, 3878–3881 (2013).
32. M. H. P. Pfeiffer, J. Liu, A. S. Raja, T. Morais, B. Ghadiani, and T. J. Kippenberg, "Ultra-smooth silicon nitride waveguides based on the damascene reflow process: fabrication and loss origins," Optica **5**, 884–892 (2018).